Ejected-electron spectrum in low-energy proton-hydrogen collisions

D. R. Schultz, C. O. Reinhold, P. S. Krstić, and M. R. Strayer
Physics Division, Oak Ridge National Laboratory, Oak Ridge, Tennessee 37831-6373
(Received 7 September 2001; published 9 May 2002)

The behavior of the ejected electron spectra resulting from low-energy ion-atom collisions relevant to momentum imaging experiments is explored and the origin of the oscillatory structures these spectra display as a function of collision energy is discussed. This is aided by consideration of the time-dependent, electronic Schödinger equation that is solved at a fixed impact parameter for 1–25 keV proton impact of atomic hydrogen utilizing the lattice, Fourier collocation technique and split-operator time propagation. At a large internuclear separation after the collision the bound states of the target and projectile are projected out for $n<4$ and the resulting continuum wave function is examined. Techniques, such as multigridding, are investigated to extend the propagation of the wave function to significantly larger final distances.

DOI: 10.1103/PhysRevA.65.052722 PACS number(s): 34.50.Fa, 34.10.+x

I. INTRODUCTION

After decades of study, the ionization of atoms by heavy-ion impact remains of significant interest from both a fundamental and an applied point of view. In the latter case, ionization is central to understanding radiation damage of solids and biological materials, and in astrophysical and laboratory plasma environments, for example, while in the former instance, there remain many outstanding issues concerning transitions into the few-body continuum. Practically as long as ionization has been studied, the most detailed investigations have relied on consideration of the so-called ejected electron spectrum, that is, the singly, doubly, or higher-order differential cross sections as a function of electron ejection angle and energy. Recent reviews by Rudd *et al.* [1] and by Stolterfoht *et al.* [2] summarize the state of knowledge regarding the ejected electron spectrum resulting from ion-atom collisions (see also [3]).

Prominent among recent discoveries have been target and projectile electron cusps, anomalous behaviors of the binary ridge of electrons, and saddle-point or top-of-barrier electron emission. For the most fundamental system, $H^+ + H$, and in a range of intermediate collision energies, relatively complete experimental and theoretical description of the ejected electron spectrum has recently been given [4,5]. For slightly more complex systems, $H^+ + He$, $He^+ + He$, and even for $H^+ + H$ at lower collision energies, very new experiments utilizing the technique of cold target recoil ion momentum spectroscopy (COLTRIMS) have presented stringent new tests of theories and of the understanding of ionization.

These recent COLTRIMS experiments [6–8] exploit techniques to produce a narrow momentum spread in the target atom source, enabling a clear momentum analysis of both the ejected electrons and ions using two-dimensional array detectors to project the extracted particles' momenta. They represent an advance towards ''complete'' experiments with the objective of measuring simultaneously as many of the free particles momenta vectors as possible in order to determine the collision dynamics at a new, very detailed level. In particular, they have identified ''sharp structures that vary strongly with impact parameter and projectile velocity'' [6] that are located near the saddle-point region, where projectile and ionized target fields balance to create a saddle in the potential experienced by the ejected electrons. Interest has especially stemmed from Olson's work that lead to the theoretical observation [9] about 20 years ago that a preponderance of the electrons emitted in relatively slow collisions (e.g., for velocities less than 1 a.u.) are more closely associated with the saddle region than with either the target or projectile ion. In fact, COLTRIMS measurements [6–8] have, in large part, sought to verify and further characterize electron emission in this region. Shortly after or concurrent with these measurements, a few theoretical models were constructed yielding seemingly contradictory explanations of the experimental findings. These theoretical approaches include the classical trajectory Monte Carlo (CTMC) technique [6,10], the uncoupled molecular Sturmian method [11], and the two-center momentum-space discretization (TCMSD) method [12,13].

The present work seeks to contribute to the resolution of the seeming theoretical contradictions and has two principal objectives. The first is to provide a general discussion of the ejected electron spectrum that is independent of any particular theoretical methodology used to compute it. Despite the very simple nature of this discussion and the fact that the basic idea is already implicit in Ref. [11], this general analysis is important because it shows that structures in the ejected electron spectrum should be expected to occur at low collision energies because a small number of magnetic substates in the continuum are usually populated. The second objective is to provide new results of exhaustive numerical simulations of the ejected electron spectra for $H^+ + H$ collisions. These were obtained utilizing techniques for direct solution of the time-dependent Schrödinger equation on a numerical lattice (LTDSE) and are extensions of earlier studies that were restricted to either collisions in two-dimensions [14] or that considered only total ionization cross sections [15]. In particular, our goal is to bring to bear a new tool to elucidate the dynamics leading to the observed low-energy oscillations of the spectrum. The present work also seeks to identify limitations of the lattice approach to describe this electronic spectrum and to explore ways in which to go beyond those limitations.

To these ends, in Sec. II we provide a fundamental view

describing the ejected electron spectrum, while in Sec. III we briefly describe the lattice approach adopted and provide details regarding its adaptation to the present study. In Sec. IV we analyze the results of our calculations of the ejected electron spectrum for collision energies between 1 and 25 keV at a fixed impact parameter and of the methods we employed to try to extend our numerical propagation to reach an asymptotic limit of the evolution. Atomic units are employed throughout unless explicitly stated otherwise.

II. THEORETICAL DISCUSSION

We shall be concerned with the scattering of a structureless projectile with charge $\mathcal{Z}_P$ by a one-electron target with a nucleus of charge $\mathcal{Z}_T$. Before the collision, the target is assumed to be at rest at the origin of the laboratory reference frame and the projectile is moving in the direction of the positive z axis with a velocity $\vec{v}_p = v_p \hat{z}$. We assume that the collision energy is large enough in comparison to the characteristic transition energies, such that we can employ a straight-line trajectory in which the time evolution of the projectile coordinate is given by $\vec{R} = \vec{b} + \vec{v}_p t$, where $\vec{b} = b\hat{x}$ is the impact parameter. The impact parameter and the collision velocity determine the collision plane, which coincides with the (x,z) plane. The Hamiltonian governing the electronic dynamics is therefore

$$\mathcal{H} = -\frac{\nabla_{\vec{r}}^2}{2} - \frac{\mathcal{Z}_T}{r} - \frac{\mathcal{Z}_P}{|\vec{r} - \vec{R}|}, \tag{1}$$

where $\vec{r}$ is the position coordinate of the electron in the laboratory frame.

Suppose now that $\Psi(\vec{r},t)$ is the electronic wave function as a function of time for a given impact parameter and collision velocity, which is obtained by solving the Schrödinger equation

$$i\frac{\partial}{\partial t}\Psi(\vec{r},t) = \mathcal{H}\Psi(\vec{r},t) \tag{2}$$

with proper initial and boundary conditions. Thus, initially, at $t \to -\infty$, the electron is in a bound state of the target, ϕ_i^T, such that $\Psi(\vec{r},-\infty) = \phi_i^T$. After the collision, at $t \to +\infty$, the wave function becomes a coherent superposition of all the bound and continuum states of the system. Provided that the time propagation is carried out to large times, the fraction of the wave function associated with ionization can be evaluated by subtracting the projection of the wave function onto all bound states,

$$\Psi_I(\vec{r},t) = \Psi(\vec{r},t) - \sum_j \phi_j^T(\vec{r})\langle \phi_j^T|\Psi(t)\rangle - \sum_j \phi_j^P(\vec{r}-\vec{R}) \times \langle \phi_j^P|\Psi(t)\rangle, \tag{3}$$

where ϕ_k^T and ϕ_k^P represent atomiclike bound states of the target and the projectile, and limit $t \to +\infty$ is assumed. The spectrum of ejected electrons [or probability density of ionized electrons in momentum space, $\rho_I(\vec{k})$] is simply given by the momentum distribution (Fourier transform) of escaping electrons in the limit $t \to +\infty$. In other words,

$$\rho_I(\vec{k}) = |\tilde{\Psi}_I(\vec{k})|^2 = \lim_{t\to+\infty} |\tilde{\Psi}_I(\vec{k},t)|^2, \tag{4}$$

where the tilde denotes a Fourier transform, $\tilde{\Psi}_I(\vec{k}) = [1/(2\pi)^3]\int d^3r \Psi_I(\vec{r},t)\exp(-i\vec{k}\cdot\vec{r})$, and $\vec{k}$ is the momentum of the ejected electron in the laboratory frame. Note that $\tilde{\Psi}_I(\vec{k},t)$ has a well-defined limit as $t \to +\infty$ whereas $\Psi_I(\vec{r},t)$ does not since the position of a continuum electron is always changing with time; classically $\vec{r} = \vec{r}(\vec{k},t)$. Alternatively, if the time integration is not carried out to infinitely long times, the spectrum of ejected electrons can be evaluated after a long but finite time by projecting the wave function onto dynamic two-center continuum states as

$$\rho_I(\vec{k}) = |\langle \phi_{\vec{k}}^-(t)|\Psi(t)\rangle|^2, \tag{5}$$

where $\phi_{\vec{k}}^-(t)$ denotes an incoming continuum state of the moving quasimolecule formed by the target and projectile Coulomb wells, which represents an escaping electron with momentum $\vec{k}$ in the limit $t \to +\infty$.

Recent momentum imaging experiments have focused on the symmetry properties of the ejected electron spectrum in the collision plane, or equivalently, the symmetry properties of

$$\rho_I(k_x,k_z) = \rho_I(k_x,k_y=0,k_z). \tag{6}$$

It has been found that, in general, the spectrum is not symmetric after a reflection in a plane normal to the x axis [i.e., $\rho_I(k_x,k_z) \neq \rho_I(-k_x,k_z)$] and, moreover, that the degree of asymmetry of the spectrum oscillates as a function of the impact parameter or the collision velocity. A reflection $k_x \to -k_x$ with respect to the k_z axis corresponds to a rotation around the k_z axis of the polar vector $\vec{k}_\perp$ by $\Delta\varphi = \pi$. Therefore, some insight can be gained by analyzing the spectrum in cylindrical coordinates k_z, $\varphi = \tan^{-1}(k_y/k_x)$, $k_\perp = \sqrt{k_x^2 + k_y^2}$. In general, the continuum wave function in the limit $t \to +\infty$ can be expanded in terms of its magnetic components as

$$\tilde{\Psi}_I(\vec{k}) = \sum_{m=-\infty}^{+\infty} \tilde{\Phi}_m(k_\perp,k_z)\exp(im\varphi), \tag{7}$$

$$\tilde{\Phi}_m(k_\perp,k_z) = \frac{1}{2\pi}\int_0^{2\pi} d\varphi\, \tilde{\Psi}_I(\vec{k})\exp(-im\varphi). \tag{8}$$

Thus, using Eq. (4), the ejected electron spectrum can be written as

$$\rho_I(\vec{k}) = \sum_{m=-\infty}^{+\infty} |\tilde{\Phi}_m(k_\perp,k_z)|^2 + \sum_{m\neq m'} \tilde{\Phi}_m(k_\perp,k_z) \times \tilde{\Phi}_{m'}^*(k_\perp,k_z)\exp[i(m-m')\varphi]. \tag{9}$$

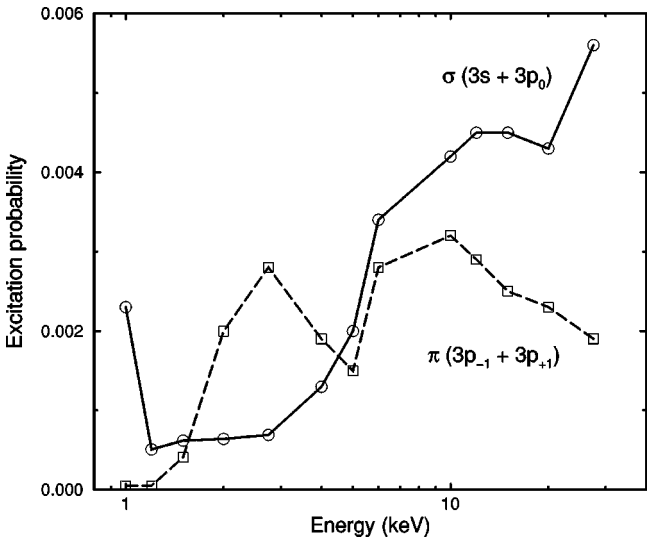

FIG. 1. Probability for populating σ $(m=0)$ and π $(m=1)$ states within the $n=3$ manifold of the target in $H^+ + H(1s)$ collisions as a function of collision energy for $b \approx 0.77$ a.u.

Note that the dependence of $\rho_I(\vec{k})$ on the polar angle φ is contained in the second sum in Eq. (9). The crossed terms in this sum are usually referred to as coherences.

As is obvious from Eq. (9), an asymmetric spectrum directly implies that the continuum wave function has at least two comparable magnetic components m and m' that differ by an odd number $[m'=m+(2j+1)$ with $j=0,\pm 1, \pm 2, \ldots]$. It is noteworthy that this property of the ejected electron spectrum is independent of any approximation method used to evaluate the spectrum. Therefore, one can conclude with certainty that any observable oscillations in the asymmetry of the spectrum is directly related to a coherence phenomenon between states with magnetic quantum numbers differing by an odd number. Furthermore, mostly low-m quantum numbers are usually populated in low-energy collisions so that the most likely origin of oscillating asymmetries involve σ $(m=0)$ and π $(m=1)$ states. To illustrate qualitatively this propensity, Fig. 1 displays the excitation probability into the $m=0$ and $m=1$ substates within the $n=3$ manifold resulting from $H^+ + H(1s)$ collisions computed in Ref. [19] for $b=0.77$ a.u. Clearly, the relative magnitude of the $m=0$ and $m=1$ populations oscillate as a function of collision energy and leads to an oscillatory behavior of the asymmetry of the $n=3$ wave function.

We note that the analysis in this section is entirely applicable to the coordinate wave function of the ejected electron as well as to the momentum wave function. Although the coordinate wavefunction can be useful in theoretical studies, it is the momentum spectrum that provides direct comparison with the COLTRIMS experiments.

Thus, the oscillatory behavior of the asymmetry of the ejected electron spectrum provides clear evidence of coherences among magnetic substates of the continuum and the changing relative transition amplitudes into these substates [i.e., the contributions with a given m value in Eq. (7)]. A possible experimental, quantitative determination of the relative importance of the magnetic substates is discussed in the Appendix. This concept can obviously apply to both classical and quantum simulations of the ejected electron spectrum. Clearly, no change in the symmetry of classical calculations can occur without changes in the relative populations of the different z components of the angular momentum, L_z of the continuum electrons. However, classical simulations should not necessarily be expected to provide accurate results because the spectrum at low energies is dominated by low quantum numbers (i.e., small m values) for which the results are farthest from satisfying the correspondence principle. Seemingly contradictory conclusions of the different theoretical simulations may not reflect discrepancies from this simple picture. Rather, they reflect the fact that the calculations are very difficult to perform and different approximations yield different amplitudes $\tilde{\Phi}_m(k_\perp, k_z)$ of the m substates. Even though the simulations in Ref. [11] are approximate, the basic idea about the relative role of the different m substates was implicitly put forth. Subsequently, more elaborate calculations were performed in Refs. [12,13]. In the following, we describe our LTDSE simulations, which provide a new complementary numerical description of the ejected electron spectrum.

III. LTDSE APPROACH AND COMPUTATIONAL CONSIDERATIONS

Recent advances in computers, numerical methods, and computational technique have opened the possibility of a new, wide range of scientific investigations, including highly accurate simulations of ion-atom collisions. One such approach has been to apply multidimensional lattice solution of partial differential equations to the few-body atomic collision problem. Motivation for pursuing a lattice, time-dependent Schrödinger equation approach stems from the goals of reaching the unbiased, numerically converged quantum mechanical result while overcoming many of the difficulties and limitations associated with other methods. For example, for low-to-intermediate energy collisions such as those considered here, well-known difficulties exist for molecular orbital close-coupling approaches involving electron translation factors and for the representation of the two-center continuum. Of course, limitations of lattice methods exist as well. However, one important advantage of LTDSE simulations is that transparent criteria can be established to analyze its convergence. Such criteria have been satisfied in the past for transitions into bound states [19]. In this work we present and analyze new calculations of the ejected electron spectrum by using this approach and discuss possible convergence criteria and extensions to be implemented in future simulations.

Typically, the TDSE is solved on a numerical lattice of finite spatial extent that necessarily has a finite number of grid points or basis elements. Therefore, when choosing a particular representation a balance must be struck between the coverage of the spatial extent of wave functions and the spatial resolution with which they are to be described. Concomitantly, choices of spatial extent and resolution have consequences for the dynamics in that the momentum resolution and range are conjugate to their spatial counterparts. These phase-space extents and resolutions impose limitations on

the physical problems that can be treated using a given lattice representation. Perhaps the greatest challenge for the LTDSE approach is to overcome what may be succinctly termed the multiscale problem in which the length or momentum scale of the wave function changes a great deal as a function of time. Examples of such a problem include excitation to Rydberg states of an atom or electron ejection. A given lattice can provide a high-fidelity representation of the initial, relatively small, atomic wave function as well as a number of excited states of the collision system, however, it cannot directly or completely represent arbitrary highly excited or continuum states whose spatial extents go beyond the boundaries of the numerical grid.

Nevertheless, the LTDSE approach can describe the time evolution of the coherent wave packet produced by the collision during which the wave function expands gradually within the boundaries of the lattice. Regarding ionization, a key ingredient to properly describe the dynamics and transitions into continuum states is an appropriate momentum space spanned by the lattice representation, which can be obtained through choice of lattice parameters and of the underlying basis representation. Here, this is accomplished using the Fourier collocation approach [18]. Advantages of this approach, and of other methods in its class, as compared to traditional grid-based methods such as finite difference schemes have come from exploiting and further developing high-order finite element and discrete variable representations (DVRs) because they can maximize the momenta represented and the fidelity of spatial derivatives [16,17] for a given spatial grid choice. Earlier work using the present approach [19] studied the excitation of low-lying states ($n<4$) of atomic hydrogen by proton impact for energies between 1 and 1000 keV, bridging the most accurate theoretical or experimental data at low, intermediate, and high energy. Accurate results were also found for excitation [20,21], charge transfer [15,20,21], and ionization [15] by using Fourier collocation, a finite difference methodology, and a pseudospectral basis function approach.

The present work is distinguished from our earlier studies in that here we seek to describe transitions into continuum states. During a collision, the portion of the electronic wave function excited to states of large target or projectile principal quantum number or emitted to the high-energy continuum leaves the Hilbert space spanned by the lattice (nearly free of reflections) via an optical potential imposed near the edge of the spatial boundary of the grid. Since after transmission through the boundary all information regarding these portions of the electronic wave function is lost, in order to calculate the spectrum associated with a particular range of the ejected electron spectrum, the time propagation must be stopped at time t before the corresponding portion of the wave function leaves the grid.

Such a limitation poses a difficult practical problem, namely, how can transition probabilities into continuum states be obtained from the wave function $\Psi(\vec{r},t)$ at the finite stopping time t? The best solution to this difficulty would be to project onto dynamic two-center continuum states as described in Eq. (5). A simplified adaptation of this method was used in Refs. [12,13]. Unfortunately, a practical and accurate scheme for computing such an overlap of the wave function and the two-center continuum is still an open problem. Therefore, a compromise had to be reached in Refs. [12,13], which was based on one-center continuum states of the target and the projectile. In order to avoid uncertainties associated with the description of the two-center continuum, in this work we evaluate transition probabilities to continuum states using Eq. (4).

To this end, we have propagated the wave function to internuclear distances larger than those in Refs. [12,13] and we focus on the portion of the electronic continuum for which it is most feasible to obtain a meaningful result: electrons emitted in the saddle region of the potential between the target and the projectile. From a classical point of view, using Eq. (4) to calculate the spectrum implicitly assumes that the momentum of the ejected electrons at the stopping time, $\vec{k}(t)$, has converged to its asymptotic value $\vec{k}(+\infty)$. Strictly speaking, sufficient conditions for this to happen are that the residual potential energy to be overcome is small compared to the kinetic energy, i.e.,

$$\frac{k^2(t)}{2} \gg \frac{\mathcal{Z}_T}{r}, \quad \frac{[\vec{k}(t)-\vec{v}_p]^2}{2} \gg \frac{\mathcal{Z}_P}{|\vec{r}-\vec{R}|}. \tag{10}$$

These conditions are, however, more severe than what is obtained practically in that near the saddle-point region the effects of the target and the projectile interactions counteract each other. In fact, the kinetic energy of an electron moving exactly with the saddle point has exactly reached its asymptotic value. Much in line with this simplified picture, our analysis of the time evolution of the momentum distribution of continuum electrons has shown that the asymmetry of the spectrum converges relatively fast in the spectral region $|\vec{k}-\vec{v}_s| \sim < v_s/2$ where $\vec{v}_s$ is the velocity of the saddle point. The present approach is not appropriate to describe other portions of the spectrum like target and projectile cusp electrons since the kinetic energies of these electrons require very large propagation distances to converge to their asymptotic energies [22]. In these regions of the ejected electron spectrum, the method adopted in Refs. [12,13] could yield more accurate results. Also, difficult to treat using the present scheme would be the component of wave function describing the high-momenta electrons, which reach the edge of the numerical grid too quickly, where they are absorbed.

The present scheme and the bounds of conveniently available computing resources combine to dictate the collision system parameters that we can currently explore. We consider $H^+ + H$ collisions with energies of 1 to 25 keV (i.e., $0.2 < v_p < 1$ a.u.), which are within the range explored in momentum imaging experiments. In the spirit of performing calculations with as few approximations as possible, we choose, as have the other recent theoretical works [6,11–13,10], to consider collisions of protons with atomic hydrogen (i.e., $\mathcal{Z}_P = \mathcal{Z}_T = 1$, $v_s = v_p/2$). No essential differences in the underlying physics is expected for this choice in comparison with experiment. For $H^+ + H$, three-dimensional lattices supporting high-order basis functions such as B splines, Chebyshev polynomials, or complex Fourier exponentials on

the order 100^3 are routinely feasible on intermediate-level computers, making it easy to run a large number of trials. Since the ionization probability falls rapidly with increasing impact parameter, we have chosen a relatively small value of this quantity to avoid numerical uncertainties in the calculation of the continuum wave function. Similarly, the overall spatial extent covered by the lattice discretization is chosen so that a sufficient separation of the projectile- and target-bound states after the collision can be reached to allow projecting out the dominant excited electronic states [i.e., Eq. (4)] but not so large that most of the ionized electrons are not still contained within the numerical box.

Thus, we utilize a Cartesian numerical grid of $135\times135\times270$ lattice points (x,y,z) corresponding to spatial dimensions of $-26<x,y<26$ a.u. and $-26<z<78$ a.u. With the target located at (0,0,0) a.u. and an impact parameter of $b=0.77$ a.u., this allows an accurate representation of bound states up to approximately $n=4$ and a reasonable separation of target and projectile $n=3$ states for a final internuclear separation of 52 a.u. The choice of a final projectile position of $x=b=0.77$ a.u., $z=52$ a.u. facilitates translation of lattice eigenstates determined for the target to the projectile position for projection operations and is symmetric (apart from the shift in x owing to the finite b) to the target's position on the grid. In particular, partial eigensolution via the Lanczos method is used to find the lowest 14 bound eigenstates of the target and are used in the calculation to project out target and projectile bound states at the end of a time propagation. We have adopted the Fourier collocation approach [18] with split-operator time propagation because of the computational speed and available shared memory parallel implementations of the fast Fourier transform, coupled with the highly accurate representation of the derivative operations Fourier expansion affords.

Thus, in this work we propagate the electronic wave function, initially in the $1s$ state of the target hydrogen atom, up to a projectile final position of $z_p=v_pt=52$ a.u. At that point, we project out the target- and projectile-bound states for $n<4$ and Fourier transform the resulting continuum portion of the wave function to produce an ejected electron momentum distribution. Depending on the impact energy, this distance is not large enough to reach a point at which the momentum wave function of continuum electrons near the saddle point region is absolutely converged. Therefore, we discuss methods to extend the propagation of the continuum wave function to larger distances, in order to obtain full convergence of the resulting momentum distribution.

IV. RESULTS AND DISCUSSION

In order to give a general impression of the characteristics of the evolution of the electronic wave function through, for example, a 5 keV $H^+ + H$ collision, we display in Fig. 2 a time sequence of contour plots representing the position probability density in the collision plane, $\rho(x,z,t)=|\Psi(x,y=0,z,t)|^2$. (We use time or the longitudinal coordinate of the projectile z_p interchangeably since they are proportional to each other: $z_p=v_pt$.) The wave function displays a roughly spherical shape early in the collision, which then elongates,

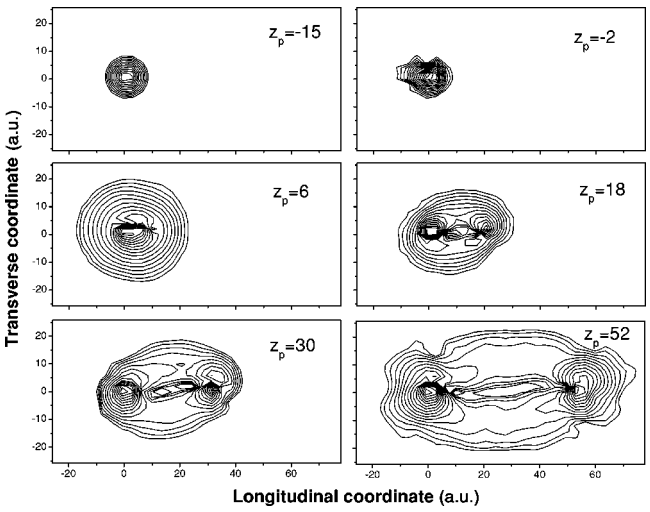

FIG. 2. Time evolution of the electronic probability density in the collision plane, $\rho(x,z,t)=|\Psi(x,0,z,t)|^2$, defined by the direction of the projectile motion $\vec{v}_p=v_p\hat{z}$ (longitudinal coordinate) and the impact parameter $\vec{b}=b\hat{x}$ (transverse coordinate), for a collision of a 5 keV proton with atomic hydrogen. The impact parameter is $b=0.77$ a.u. and the frames correspond to projectile longitudinal coordinates $z_p=-15,\ -2,\ 6,\ 18,\ 30$, and 52 a.u.

stretching between the target and projectile afterwards. One may readily note the roughly equal amounts of density centered on both the target and projectile, and the bipolar shape of the density that will end up in the continuum. In particular, for this b and v_p, very little density moves along the line connecting target and projectile, including the saddle point, but rather lies on either side of this line. This simple observation is somewhat in contradiction with very early ideas of saddle-point electron emission, which envisioned electrons ''surfing'' on the top of the saddle.

Another way to view the time evolution of these features near the saddle with many more time slices but still within a two-dimensional picture is to plot a sequence of slices transverse to the direction of projectile motion (i.e., along $\vec{b}$, the x direction) through the midpoint between the target and projectile,

$$\rho(x,t)=\int_{z_p/2-\delta z}^{z_p/2+\delta z}dz\,\rho(x,z,t) \tag{11}$$

$$=\int_{z_p/2-\delta z}^{z_p/2+\delta z}dz\,|\Psi(x,y=0,z,t)|^2, \tag{12}$$

where $\delta z\ll z_p/2$. Figure 3 depicts the time evolution of $\rho(x,t)$ for 20 keV $H^+ + H$. The top portion of Fig. 3 maps a very dense sequence of these time slices of the probability density in the collision plane for given projectile longitudinal coordinates. A bipolar distribution is also present in this case, but with significant asymmetry towards the negative side of the x axis, which is opposite to the direction of $\vec{b}$. The bipolar feature develops rather suddenly at about $z=10$, and then the two peaks of the transverse slice move to larger transverse coordinates very slowly as they also gradually broaden.

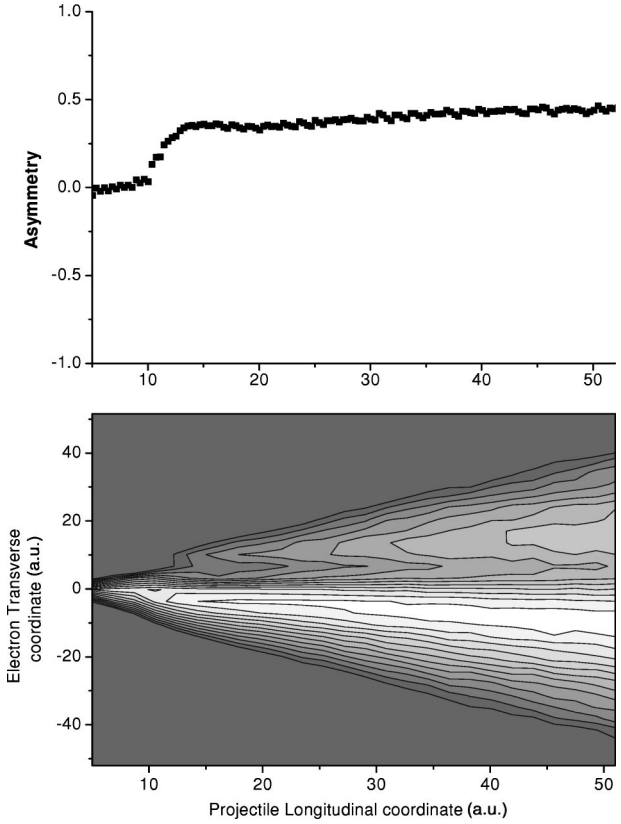

FIG. 3. Time evolution of the transverse projection of the electronic probability density at the midpoint between the projectile and the target, $\rho(x,t)=\rho(x,z=z_p/2,t)=|\Psi(x,0,z=z_p/2,t)|^2$, as a function of the projectile longitudinal position $z+p=v_pt$ after the collision (i.e., $z_p>5$ a.u.). The collision energy is 20 keV and $b=0.77$ a.u.The upper portion of the figures displays the asymmetry of the distribution as a function of internuclear separation, as described in the text.

The data in the figure illustrate a typical collision energy for which convergence of the asymmetry of the spectrum is reached in the region of the saddle. In other words, the degree of asymmetry of the wave function,

$$A(t)=\frac{\int_0^{+\infty}dx\rho(x,t)}{\int_{-\infty}^{0}dx\rho(x,t)}, \tag{13}$$

converges very rapidly as a function of time. For the distribution at 20 keV, even the simple approximation $A'(t)=(P_+-P_-)/(P_++P_-)$, where $P_{+,-}$ is the height of the peak on the $+x$ or $-x$ side, illustrates the rapid convergence, as also shown in Fig. 3.

In Fig. 4 (top) we display again the final time frame of the sequence shown in Fig. 2, that is, the electronic probability density in the collision plane for 5 keV $H^+ + H$ at $z_p=52$ a.u. Also shown is the continuum probability density, $\rho_I(x,t)=|\Psi_I(x,0,z=z_p/2,t)|^2$, where Ψ_I is defined as in Eq. (3) after 14 lattice-bound eigenstates $[H(1s\text{-}3d)]$ have been projected out at the target and projectile positions. Some density

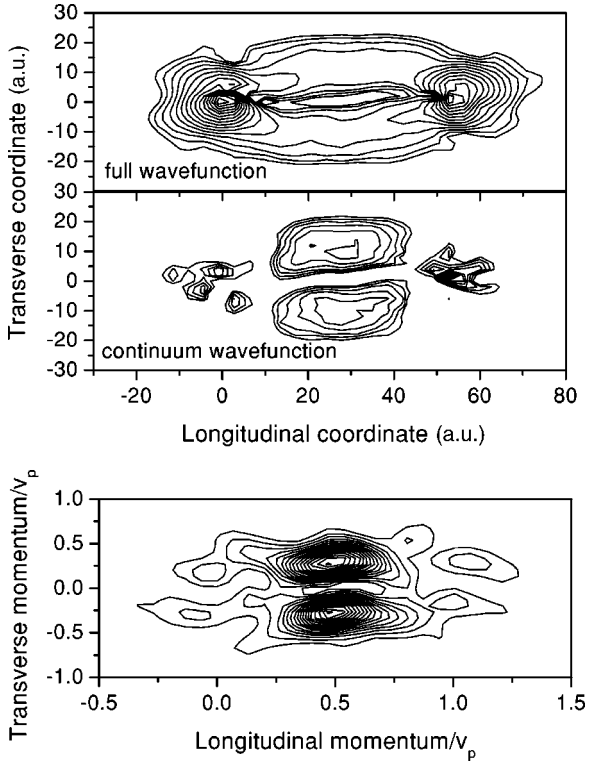

FIG. 4. Analysis of the final electronic state of the collision for 5 keV $H^+ + H$ at a final longitudinal internuclear separation of $z_p=52$ a.u. for $b=0.77$ a.u. The uppermost frame displays the total electronic probability density in the collision plane, $\rho(x,z)$. The middle frame displays the corresponding continuum density $\rho_I(x,z)$ obtained after target and projectile bound states for $n<4$ have been projected out. The lower frame displays the continuum probability density in momentum space, $\rho_I(k_x,k_z)$, obtained from the Fourier transform of the continuum wave function.

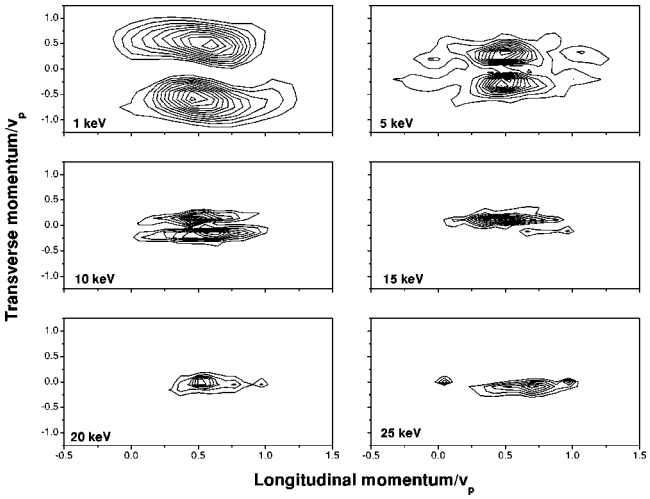

FIG. 5. The electronic momentum distribution of ionized electrons in the collision plane, $\rho_I(k_x,k_z)$, for $H^+ + H$ collisions and various collision energies after the time propagation is carried out to a longitudinal internuclear distance $z_p=52$ a.u. for $b=0.77$ a.u.

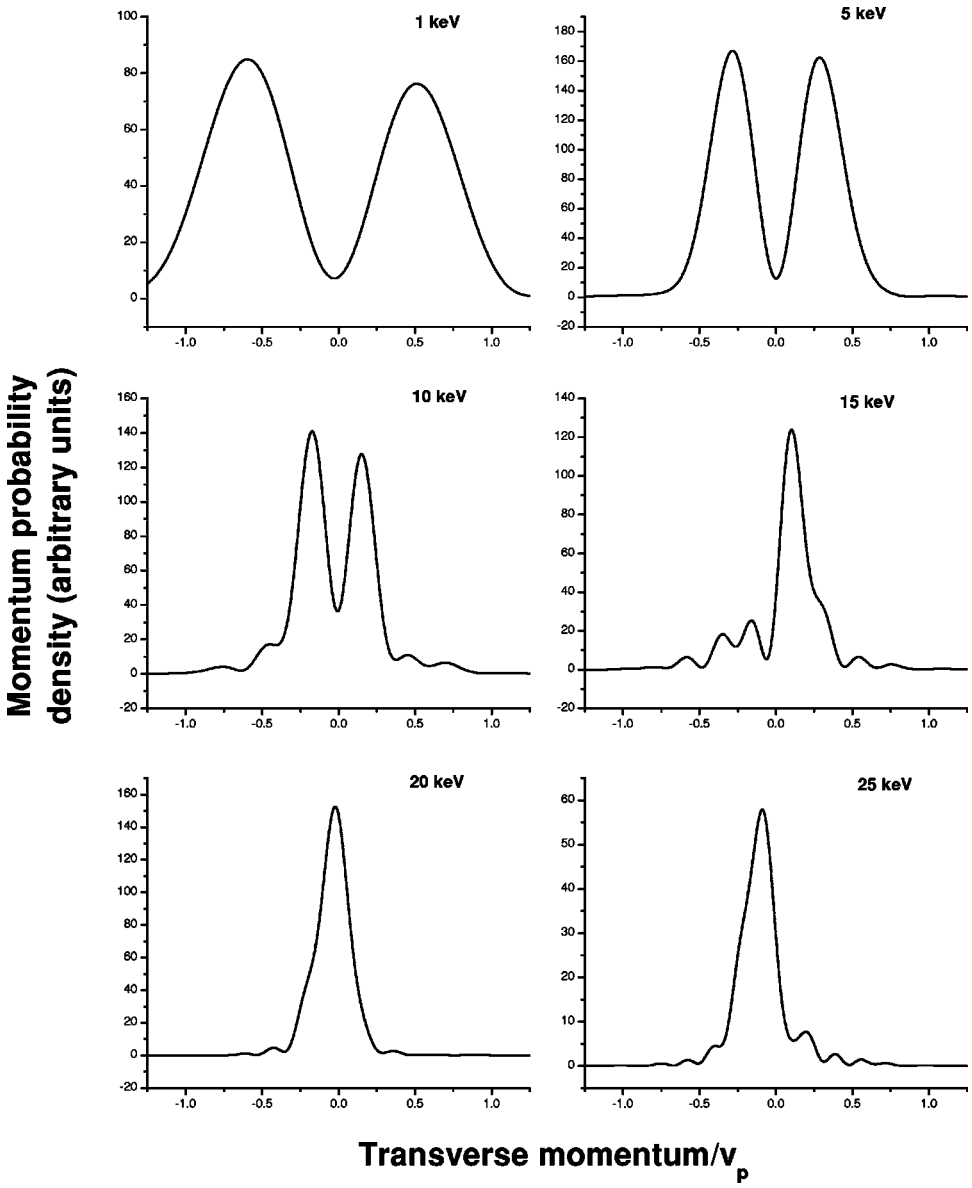

FIG. 6. Transverse projections of the electronic momentum distribution, $\rho_I k_x$, for 1–25 keV $H^+ + H$ for $b = 0.77$ a.u.

remains near the target and projectile positions, possibly bound states of higher n and/or low-lying continuum states of these centers (i.e., cusp electrons). However, the most significant feature of the continuum density are the prominent structures centered close to $z = z_p/2 = 26$ a.u. In Fig. 4 (bottom) we display the spectrum of ejected electrons in the collision plane [i.e., the probability density in momentum space defined in Eq. (6)]. As is customary in momentum imaging experiments, the momentum scales have been normalized to the projectile velocity. Even though the wave function has been propagated up to a finite internuclear distance, a significant degree of its most complex evolution has taken place signified by the fact that the spatial and momentum distributions are quite similar in shape. The spectrum of ejected electrons is nearly symmetric with respect to the k_z axis, indicating that it is most likely dominated by a single magnetic quantum number. The bipolar shape of the spectrum resembles that of a $m = 1$ (π) orbital.

The momentum distribution of continuum electrons calculated in this way for 1, 5, 10, 15, 20, and 25 keV proton impact is shown in Fig. 5. A strongly π-like distribution is seen for the lowest energies whereas for the highest energies a peak only on the side opposite to the direction of $\vec{b}$ remains. This is seen even more clearly in Fig. 6 that displays a slice of the transverse momentum density in the collision plane at a longitudinal momentum halfway between that of the target ($k_z/v_p = 0$) and the projectile ($k_z/v_p = 1$),

$$\rho_I(k_x) = \int_{v_p/2-\delta k_z}^{v_p/2+\delta k_z} dk_z \rho_I(k_x, k_z) \tag{14}$$

$$= \int_{v_p/2-\delta k_z}^{v_p/2+\delta k_z} dk_z |\tilde{\Psi}_I(k_x, k_y = 0, k_z)|^2, \tag{15}$$

where $\delta k_z \ll v_p/2$. The rapid change with impact energy of the shape and "up/down" asymmetry [e.g., Eq. (13)] of these

distributions are the most intriguing aspects of the ejected electron spectrum first found in COLTRIMS experiments [6,8].

Previously, the TCMSD method [12,13] was applied to investigate the v_p dependence of the oscillations of the momentum distribution for 5–100 keV $H^+ + H$ at an impact parameter of $b = 1.2$ a.u. The time propagation was carried out to some finite value of final internuclear separation, as in the present work, determined by computational constraints. A typical calculation for a given impact paramenter and a given collision velocity is still quite demanding computationally. At the lowest collision energy presented in this paper such time propagation takes more than 10 h using a Cray J-90 or Silicon Graphics Power Challenge computer with 4–16 processors. Since the present calculations were performed for a different impact parameter, $b = 0.77$ a.u., a detailed comparison is not possible. However, a few noticeable differences are clearly observed concerning $\rho_I(k_x)$. First, the double-peaked structures at low collision energies are found to be considerable sharper than those reported in Ref. [10] (i.e., the minimum at $k_x = 0$ in this work is considerably deeper). Second, our results in Fig. 6 exhibit a rapid change in asymmetry from side to side in the collision energy range between 15 keV, and 25 keV, which is not present in Ref. [10]. These differences might be easily explained by the changing behavior with impact parameter of the relative importance of π and σ or other magnetic substates in the spectrum of ejected electrons.

Given the ultimate goal of making a quantitative comparison with momentum imaging experiments, let us summarize the status of the theoretical development so far, and list what needs to be carried out to reach this goal. To begin with, all of the experimental and theoretical works described have confirmed the very basic concept that electron emission associated with the saddle region is of great importance in the overall view of low-energy ionization. After the experimental observation of oscillations of the peaks in the transverse momentum distribution, a fundamental theoretical picture based on changing coherences among the magnetic substates of the continuum has emerged. *Ab initio* numerical calculations, TCMSD, and LTDSE have yielded results in qualitative agreement but need to be extended. Specifically, the most significant present constraint is the difficulty these approaches have in propagating the electronic wave function to large final distances, described above as the multiscale problem. It would be straightforward to compare the various theoretical results as a function of b, v_p, and final z_p, for consistency. Finally, both approaches would have to be elaborated to treat the more-than-one-electron systems examined experimentally (e.g., $He^+ + He$) or experimentalists would have to be motivated to repeat their measurements for $H^+ + H$.

In the present work, we have sought pathways to go beyond what we see as the most significant of these challenges, that is, how to properly propagate the wave function to an asymptotic form in order to describe the entire ejected electron spectrum. The methods that we envision are based on separation of the time evolution into different time intervals, the first of which is solved fully quantally, as in the LTDSE calculations described above. Subsequently, the output of the first region is used as the initial wave function for the second time interval after projecting out the bound states that are expected to become decoupled from all other reaction channels (i.e., low-lying energy levels of the target and the projectile). The basic idea behind this scheme is that after projecting out many ''inner region'' states, the smaller, most quantal portions of the resulting wave function are removed. The initial wave function for the second time interval should have a larger scale and, therefore, could be properly described on a new grid with larger spatial extent and larger spatial step that uses the same computational resources as the original grid.

This procedure could be repeated a few times for various consecutive time intervals and is usually called multigridding. We note, however, that such multigridding procedure has to be carried out with extreme care. That is, given a particular finite element or DVR choice, there exists a maximum spatial or momentum grid spacing at which resolution (spatial or momentum) exists to support the relevant character of the wave function and Hamiltonian. Therefore, to increase the spatial extent of the lattice, one cannot simply increase the grid spacing in order to represent dynamics on one scale without losing resolution of the dynamics on other pertinent scales. Most compatible with the numerical and computational methods we have employed is to devise a scheme by which the wave function can be re-discretized on a new grid of larger spatial extent that satisfies the requirements of sufficient spatial and momentum resolution. Alternative strategies exist, such as the choice of a nonuniform grid space, compatible with other lattice methods.

We have explored this approach by using the wave function propagated to $z_p = 52$ a.u. and with the $n < 4$ bound target and projectile states projected out to seed propagation of the remaining continuum wave function to larger z_p. In particular, we take the complex value of the wave function at every other lattice point on this first grid and use it as the starting wave function on a grid with the same number and distribution of grid points with twice the spatial extent in each coordinate. We then run the quantal, split operator time propagation on this regridded wave function to a distance of $z = 104$ a.u. at which point the momentum distribution is computed as before. The projecting out of the bound states, and the absorption of the fast moving electronic density at the boundaries, remove the majority of the high momentum content of the wave function. This makes the propagation on the larger grid feasible even though, having eight times the spatial volume with the same number of lattice points (basis functions), it has a lower maximum momentum that it can support. Also, once the bound states are removed, the wave function varies with a longer wavelength scale and it is, thus, spatially represented better on the larger but coarser grid than it would be with the smaller, more spatially varying bound states present.

For the higher impact energies considered for which case the ionization probability is relatively large by $z_p = 52$ a.u., this regridding was successfully implemented. In Fig. 7 we display the same momentum distribution for 20 keV proton impact as was shown in Fig. 5, and below it, the momentum

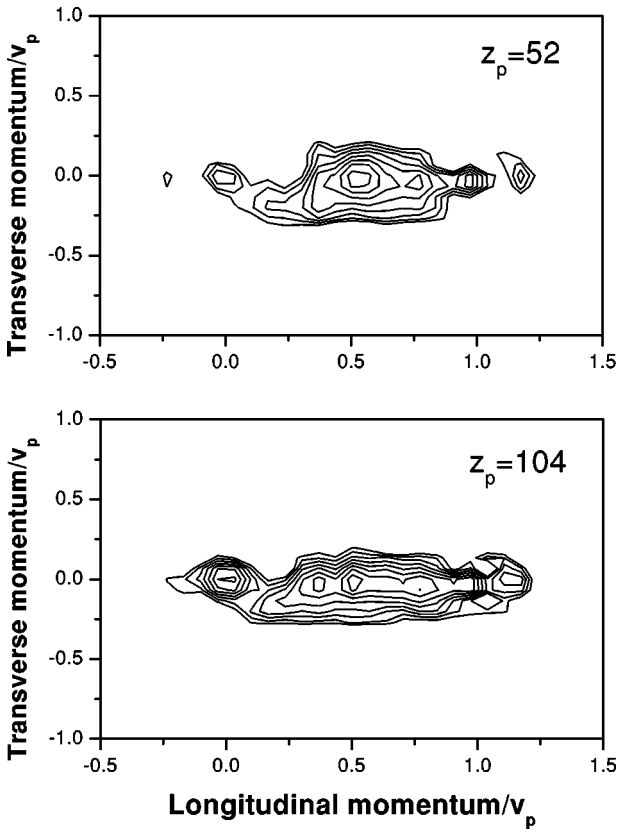

FIG. 7. The electronic momentum distribution for $b=0.77$ a.u. after bound state projection for 20 keV $H^+ + H$ at $z_p=52$ a.u. (upper frame) and after regridding and time propagation of the wave function on a numerical lattice with dimensions twice as large and up to $z_p=104$ a.u. (lower frame).

distribution found after regridding and propagation to $z_p=104$ a.u. The same general shape of the distribution is preserved in this propagation, but the transverse momentum spread narrows and the longitudinal spread elongates, as expected. One can also note from the larger grid results that the target- and projectile-centered momentum density increases with long propagation, indicating the postcollisional evolution of these features as well. For the smaller impact energies considered here, the multigridding procedure has not yet been successfully implemented because of numerical difficulties associated with the small magnitude of the continuum wave function.

We have also considered the possibility of performing the propagation of the wave function after the first time interval using classical mechanics. Motivation for this approach stems from the general success of the CTMC method in describing the features of differential ionization cross sections for intermediate energy ion-atom collisions, and from the fact that at a certain internuclear separation, an ejected electron should simply evolve classically once its de Broglie wavelength becomes short compared to this separation. Chassid and Horbatsch [23] have recently performed a similar exploration in a one-dimensional model of ion-atom collisions. The basic procedure we considered was to convert the electronic wave function at the conclusion of the LTDSE time propagation (after bound-state projection) into a classical distribution of test particles in phase space (probability packets). Subsequently, each test particle is propagated, as in the CTMC method, to a very large final internuclear distance by solving Hamilton's equation of motion (or equivalently, the classical Liouville equation for the whole probability density in phase space). By binning in angle and energy the test particles, weighted by the probability density carried by each, the asymptotic momentum distribution can be straightforwardly computed.

Even though such a procedure can be implemented, we found that, in the spirit of performing calculations with as few approximations as possible, clear limitations arise at low collision energies due to the impossibility of mapping with good resolution all the quantum structures into classical phase space. The mapping of a quantum wave function $|\Psi(t)\rangle$ onto a classical positive definite probability density, in phase space, $\rho_C(\vec{r},\vec{k},t)$, is not unique. One of the simplest mappings that we considered is called the Husimi distribution [24] and is given by

$$\rho_C(\vec{r},\vec{k},t)=|\langle G_{\vec{r},\vec{k},s}|\Psi(t)\rangle|^2, \tag{16}$$

where $|G_{\vec{r},\vec{k},s}\rangle$ is a minimum uncertainty Gaussian wave packet describing a free electron centered at $\vec{r}$ and moving with an average momentum $\vec{k}$. The squeezing parameter s represents the width of the Gaussian in the position coordinate (the width in momentum is $1/s$) and can be tuned to resolve better either the momentum or the position coordinate of the electron. The Husimi projection in Eq. (16) resembles a procedure of attempting to measure the position and the coordinate of the electron within the limitations of the uncertainty principle and using a resolution s for the position and a resolution $1/s$ for the momentum. The main difficulty associated with low-energy ion-atom collisions is that this quantum-classical mapping partially ''washes out'' structures of the continuum wave function because, at the final internuclear separation considered here, $z_p=52$ a.u., the product of the widths of the structures in the position and momentum distributions is very close to the Planck's constant (i.e., $\Delta x \Delta k_x / v_p \sim 1/v_p$). This limitation is clearly visible in the position and momentum distributions depicted in Fig. 4 for a collision energy of 5 keV. Thus, we conclude that significantly larger internuclear separations must be reached before the quantum-classical mapping is performed without much loss of information. Moreover, the internuclear distance at which the mapping should be performed increases as $1/v_p$ for decreasing collision velocities.

V. SUMMARY

We have studied the behavior of the ejected electron spectra resulting from low-energy ion-atom collisions, presenting a general analysis, not dependent on the approximations used, of the origin of oscillatory structures in momentum imaging spectra in order to clarify that such structures are a direct consequence of coherences among the various magnetic substates in the continuum. Utilizing the lattice, Fourier

collocation method, we have solved the time-dependent Schrödinger equation for 1–25 keV $H^+ + H$ collisions at a fixed impact parameter to examine the variations of the momentum distribution of the ejected electron spectrum in the saddle-point region with the projectile energy. Our results confirm the general conclusions drawn previously by other authors.

Future directions of research need to focus on schemes of time propagation to reach larger internuclear separations in order to reach fully converged spectra. Possible pathways to extend the time propagation to asymptotic form such as lattice regridding and classical postpropagation were investigated and their limitations discussed. Accomplishing this reliably will be key in future work to compare results of this and similar methods directly and quantitatively with experimental measurements. Some success in regridding was found for cases in which the ejected electronic probability density was not too diffuse to allow the regridding to map the wave function over to the new grid with sufficient fidelity. Reliable classical postpropagation at the present stopping distance is not possible owing to the inability to map precisely the quantum wave function onto a phase-space probability density. A tour de force calculation in which fully quantal methods used within an inner spatial zone, with possible multigridding or adaptive-gridding, and an outer classical mechanical propagation, is needed. At that point, not only will the *ab initio* quantal approaches be able to explore qualitatively the oscillations of the low-energy ejected electron spectrum, but also reach quantitative comparison with experiment for the fundamental $H^+ + H$ collision system.

ACKNOWLEDGMENTS

The authors gratefully acknowledge support through grants from the US DOE Office of Fusion Energy Sciences and Office of Basic Energy Sciences to Oak Ridge National Laboratory, which is managed by UT-Battelle, LLC, under Contract No. DE-AC05-00OR22725.

APPENDIX: ANALYSIS OF THE RELATIVE MAGNETIC CONTRIBUTIONS

The analysis made in Sec. II for $k_y = 0$ can be generalized. To see this we consider the distribution in the plane $k_y = K_y = \text{const}$, parallel to the collision plane $k_y = 0$. A reflection $k_x \rightarrow -k_x$ corresponds to rotation of the momentum vector (k_x, K_y, k_z) with polar angle $\varphi_Y = \tan^{-1}(K_Y/k_x)$ into the vector $(-k_x, K_y, k_z)$ with polar angle $\varphi_Y' = \pi - \varphi_Y$ and,

$$\rho_I(\pm k_x, K_y, k_z) = \sum_{m=-\infty}^{+\infty} |\tilde{\Phi}_m(k_\perp, k_z)|^2 + \sum_{m-m'=even} \tilde{\Phi}_m(k_\perp, k_z)\tilde{\Phi}^*_{m'}(k_\perp, k_z) \times \exp[\pm i(m-m')\varphi_Y] \pm \sum_{m-m'=odd} \tilde{\Phi}_m(k_\perp, k_z)\tilde{\Phi}^*_{m'}(k_\perp, k_z) \times \exp[\pm i(m-m')\varphi_Y]. \quad \text{(A1)}$$

Clearly, all magnetic components contribute to the spectrum asymmetry for $K_y \neq 0$. The momentum imaging experiments have been restricted to the collision plane where $\varphi_Y = 0$ but can be generalized and an interesting application emerges from this general formula.

If one assumes that only σ and π magnetic substates are present in the electron spectrum, then a measurable asymmetry parameter for a given $(k_\perp, k_z)$ is

$$A_Y = \rho_I(k_x, K_y, k_z)/\rho_I(-k_x, K_y, k_z) = \frac{1 + 2R^2_{\sigma\pi} + 2R_{\sigma\pi}\cos(\Delta\phi_{\sigma\pi} + \varphi_Y)}{1 + 2R^2_{\sigma\pi} - 2R_{\sigma\pi}\cos(\Delta\phi_{\sigma\pi} - \varphi_Y)}, \quad \text{(A2)}$$

where

$$R_{\sigma\pi} = R_{\sigma\pi}(k_\perp, k_z) = |\tilde{\Phi}_\pi(k_\perp, k_z)|/|\tilde{\Phi}_\sigma(k_\perp, k_z)|$$

and

$$\Delta\phi_{\sigma\pi} = \Delta\phi_{\sigma\pi}(k_\perp, K_y, k_z) = \arg[\tilde{\Phi}_\sigma(k_\perp, k_z)] - \arg[\tilde{\Phi}_\pi(k_\perp, k_z)].$$

.

If future COLTRIMS experiments would allow the momentum imaging in the planes $K_y \neq 0$, parallel to the collision plane, one would be able to experimentally determine both relative magnitudes and phases of the different magnetic components of the continuum electron wave functions. This would provide an unprecedented, in-depth view of the ionization spectrum. In the above example involving two magnetic substates, momentum imaging in only one additional plane $K_y \neq 0$ is required for determination of $R_{\sigma\pi}$ and $\Delta\phi_{\sigma\pi}$. While this procedure would most likely suffice at low collision energies, it can be easily generalized to larger collision energies where a larger number of active magnetic components are involved by increasing the number of planes in which the spectrum is measured.

[1] M.E. Rudd, Y.-K. Kim, D.H. Madison, and T.J. Gay, Rev. Mod. Phys. **64**, 441 (1992).

[2] N. Stolterfoht, R.D. DuBois, and R.D. Rivarola, *Electron Emission in Heavy Ion-Atom Collisions* (Springer, Berlin, 1997).

[3] D. R. Schultz, C. O. Reinhold, and R. E. Olson, in *Two-center Effects in Ion-atom Collisions*, edited by T.J. Gay and A.F. Starace, AIP Conf. Proc. No. 362 (AIP, Woodbury, NY, 1996).

[4] M.W. Gealy, G.W. Kerby, Y.-Y. Hsu, and M.E. Rudd, Phys. Rev. A **51**, 2247 (1995).

[5] G.W. Kerby, M.W. Gealy, Y.-Y. Hsu, M.E. Rudd, D.R. Schultz, and C.O. Reinhold, Phys. Rev. A **51**, 2256 (1995).

[6] R. Dörner, H. Khemliche, M.H. Prior, C.L. Cocke, J.A. Gary, R.E. Olson, V. Mergel, J. Ullrich, and H. Schmidt-Böcking, Phys. Rev. Lett. **77**, 4520 (1996).
[7] M. Abdallah, S. Kravis, C.L. Cocke, Y. Wang, V.D. Rodriguez, and M. Stöckli, Phys. Rev. A **56**, 2000 (1997).
[8] M.A. Abdallah, C.L. Cocke, W. Wolff, H. Wolf, S.D. Kravis, M. Stöckli, and E. Kamber, Phys. Rev. Lett. **81**, 3627 (1998).
[9] R.E. Olson, Phys. Rev. A **27**, 1871 (1983); **33**, 4397 (1986).
[10] E.Y. Sidky, C. Illescas, and C.D. Lin, Phys. Rev. Lett. **85**, 1634 (2000).
[11] J.H. Macek and S. Yu.Ovchinnikov, Phys. Rev. Lett. **80**, 2298 (1998).
[12] E.Y. Sidky and C.D. Lin, J. Phys. B **31**, 2949 (1998).
[13] E.Y. Sidky and C.D. Lin, Phys. Rev. A **60**, 377 (1999).
[14] P. Gavras, M.S. Pindzola, D.R. Schultz, and J.C. Wells, Phys. Rev. A **52**, 3868 (1995).
[15] A. Kolakowska, M.S. Pindzola, and D.R. Schultz, Phys. Rev. A **59**, 3588 (1999).
[16] A.S. Umar, J. Wu, M.R. Strayer, and C. Bottcher, J. Comput. Phys. **93**, 426 (1991).
[17] J.C. Wells, V.E. Oberacker, M.R. Strayer, and A.S. Umar, Int. J. Mod. Phys. C **6**, 143 (1995).
[18] J.C. Wells, D.R. Schultz, P. Gavras, and M.S. Pindzola, Phys. Rev. A **54**, 593 (1996).
[19] D.R. Schultz, M.R. Strayer, and J.C. Wells, Phys. Rev. Lett. **82**, 3976 (1999).
[20] A. Kolakowska, M.S. Pindzola, F. Robicheaux, D.R. Schultz, and J.C. Wells, Phys. Rev. A **58**, 2872 (1998).
[21] X-.M. Tong, D. Kato, T. Watanabe, and S. Ohtani, Phys. Rev. A **62**, 052701 (2000).
[22] C.O. Reinhold and R.E. Olson, Phys. Rev. A **39**, 3861 (1989).
[23] M. Chassid and M. Horbatsch, J. Phys. B **31**, 515 (1998).
[24] K. Husimi, Proc. Phys. Math. Soc. Jpn. **22**, 264 (1940).